American Mineralogist, Volume 96, pages 383–392, 2011

High-pressure structural evolution and equation of state of analbite

Nadia Curetti,[1,*] Lindsay M. Sochalski-Kolbus,[2] Ross J. Angel,[2] Piera Benna,[1] Fabrizio Nestola,[3] and Emiliano Bruno[1]

[1]Dipartimento di Scienze Mineralogiche e Petrologiche, Università di Torino, Via Valperga Caluso 35, I-10125 Torino, Italy
[2]Virginia Tech Crystallography Laboratory, Department of Geosciences, Virginia Tech, Blacksburg, Virginia 24060, U.S.A.
[3]Dipartimento di Geoscienze, Università di Padova, Via Giotto 1, I-35137 Padova, Italy

Abstract

The volume and unit-cell parameters of analbite (i.e., $NaAlSi_3O_8$ with complete Al,Si disorder) have been determined by single-crystal X-ray diffraction to a maximum pressure of ~8.71 GPa. The volume variation with pressure is described by a fourth-order Birch-Murnaghan equation of state with K_{0T} = 50.3(5) GPa, K_0' = 8.9(5), and K_0'' = –2.4(3) GPa^{-1}. The value of the room-pressure bulk modulus is ~4% lower than that of low albite, and the onset of volume softening in analbite is at ~6.7 GPa, some 1.7 GPa higher than the onset in albite. The anisotropy of compression of analbite is less than that in albite.

Single-crystal structure determinations of analbite to ~9.4 GPa show that there is no significant detectable compression of the T-O bonds within the structure, and the compression of the framework of tetrahedra is therefore accommodated by changes in the T-O-T angles, which result in significant compression of the "crankshaft chains" within the framework. No significant shear of the tetrahedral rings of analbite was detected, in contrast to the structural compression of albite. Overall, the structural changes that occur in analbite from 0.0001 to 9.4 GPa resemble those seen in ordered albite over the pressure range 0.0001–4 GPa. Therefore analbite shows a significantly greater structural rigidity than low albite up to pressures of 9.4 GPa.

Keywords: Analbite, equation of state, high pressure, X-ray structure, single crystal

Introduction

The quantity of high-quality structural data on the compression of feldspars remains extremely limited and so "understanding the interplay of compositional change and Al,Si order in determining the elastic and high-pressure response of alkali feldspars requires further detailed study of several compositions, including structural determinations of the disordered end-members at high-pressures" (Nestola et al. 2008). To that end, only the structure of low albite has previously been determined at high pressures (Downs et al. 1994; Benusa et al. 2005), and there has been no data on the structural evolution with pressure of completely disordered albite (analbite); the recent study of Tenner et al. (2007) was limited to the determination between 0.0001 and 7.6 GPa of the unit-cell parameters. For a more complete review of the effects of pressure on the feldspar group of minerals the reader is referred to Angel (1994), Downs et al. (1994), Ross (2000), Benna et al. (2007), and Nestola et al. (2008).

For ordered low albite, Downs et al. (1994) observed that in the pressure range 0.0001–4 GPa the Si-O-Si angles either increase or remain constant while only the Al-O-Si angles decrease. The authors concluded that the compression is accomplished through the bending of the Al-O-Si angles that squeeze together the chains of four-membered rings that run parallel to [001], and so compress the "crankshaft chains" of tetrahedra within the structure. At higher pressures, between 3.8 and 6.5 GPa, Benusa et al. (2005) observed the beginning of a significant softening of the structure and attributed it to a tilting of the T1 tetrahedra around the [001] direction and shear of the four-membered rings. The initiation of these structural changes appeared to be correlated with the beginning of the decrease in bulk modulus observed at 5 GPa. Above 5 GPa the bulk modulus progressively decreases and, above 8.4 GPa, low albite is softer than at room pressure.

We have now carried out an investigation of the high-pressure behavior of analbite, that is albite with a disordered distribution of Al and Si, to determine the effects of disordering on the bulk modulus and the mechanisms of compression of albite.

Experimental methods

The crystals of albite studied in the present work are from Champorcher, Aosta Valley, Italy. The chemical analyses of several crystals were performed with a Cambridge S-360 SEM with Oxford Link EDS instrument. The composition was close to pure albite ($Na_{0.99}Al_{1.01}Si_{2.99}O_8$) (K and Ca, if present, were below the detection limit of the instrument). Both the T-O bond lengths obtained from structural refinement and the unit-cell parameters indicated complete Al,Si ordering (Table 1) in the natural sample (space group $C\bar{1}$). The crystals of low albite were then annealed in an electric furnace at T = 1000 °C in air for 31.5 days. After this thermal treatment, structure refinement indicated only partial Al,Si disorder, so the same crystals were further annealed at T = 1060 °C for 28 days. After this second thermal treatment the crystals of albite showed complete Al,Si disorder (Table 1), and are thus correctly termed "analbite" (Smith and Brown 1988). All of these room-pressure intensity data collections and the HP data collections on analbite were performed by single-crystal X-ray diffraction with a Gemini R Ultra diffractometer (Oxford Diffraction) equipped with CCD detector, using monochromatic Mo$K\alpha$ radiation and the tube operating at 50 kV and 40 mA (CrisDi Centre, University of Turin).

For determination of the evolution of the unit-cell parameters under pressure,

* E-mail: nadia.curetti@unito.it

a single crystal of analbite was loaded in an ETH-type diamond anvil cell (DAC, hereafter) (Miletich et al. 2000) along with a quartz crystal and a ruby chip. The dimensions of the analbite and quartz crystals are $160 \times 160 \times 36$ and $80 \times 50 \times 30$ μm^3, respectively. The stainless steel gasket used to hold the crystals was indented to a thickness of 80 μm and drilled to a diameter of 300 μm. The piece of quartz was used as a pressure standard and a ruby chip was used to measure approximate pressure. The cell was loaded with a 4:1 methanol:ethanol solution to ensure hydrostatic conditions. The unit-cell parameters at each pressure point were determined using a least-squares fit to the positions of between 20–34 reflections for the analbite and 11–16 reflections for the quartz determined by the 8-position centering technique (King and Finger 1979) on a Huber 4-circle diffractometer with unfiltered Mo$K\alpha$ radiation in a 2θ range of ~10 to ~30°. The unit-cell volume of quartz was used with the equation of state (EoS) of Angel et al. (1997) to determine the pressure for each data point up to 8.710(8) GPa. EoS parameters for analbite were determined by a least-squares fit (Angel 2000) to the *P-V* data. The pressures and unit-cell parameters determined for analbite are given in Table 2.

In a separate experiment another crystal of analbite with dimensions $113 \times 185 \times 39$ μm^3 was selected for high-pressure structural studies and loaded in an ETH-type DAC for intensity data collection up to 9.4 GPa. The (010) plane normal of the crystal was approximately parallel to the axis of the DAC. A foil of T301 steel 250 μm thick was used as a gasket and was pre-indented to 110 μm before drilling a hole by spark-erosion (∅ 250 μm). A 16:3:1 mixture of methanol:ethanol:water was used as pressure-transmitting medium. The internal pressure was determined with a Horiba Jobin micro-Raman spectrometer (Scansetti Centre, University of Turin) from the shift of the fluorescence line of four rubies scattered in the sample chamber of the DAC. The uncertainty on *P* was estimated to be about 0.1 GPa (Mao et al. 1986). Intensity data were collected at room conditions in the DAC (without pressure-transmitting medium) and at *P* = 1.2, 3.2, 5.5, 7.2, 8.0, 9.0, and 9.4 GPa (Table 3). A total of 1783 frames (frame width 0.2°, exposure time 60 s, detector-sample distance 80 mm) were collected at each pressure in 4 φ- and 12 ω-scans, covering all of the accessible reciprocal space. The CrysAlis Red program (Oxford Diffraction) was used to integrate the intensity data, and the Absorb-6.0 program (Angel 2004) was used to correct for absorption and gasket shadowing. Structure refinements using the ShelX-97 package (Sheldrick 2008) were done in space group $C\bar{1}$ at all pressures as no violations of this symmetry were found. To reduce the number of refined parameters, the structure refinements at all pressures were carried out with isotropic displacement factors for T- and O-sites. However, the Na position in albite is extremely anisotropic (Quareni and Taylor 1971; Winter et al. 1977) and refinements will not converge properly with an isotropic model. In analbite, this anisotropy is increased by the different environments around the Na atom as a result of the Al/Si disorder (Winter et al. 1979). Therefore the Na-site was modeled as anisotropic at all pressures. A comparison between the refinement to the room-pressure data set collected in the DAC and that determined from the full data set in air shows that the refined displacement parameters of the Na atom are identical within the e.s.d. values. Therefore the refined anisotropy of the Na atom is not significantly affected by the restricted access to reflections in the DAC. Unit-cell

TABLE 1. Unit-cell parameters and mean <T-O> bond distances for untreated albite from Champorcher and for thermally treated albite (e.s.d. values in parentheses)

T (°C)	*t* (h)	*a* (Å)	*b* (Å)	*c* (Å)	α (°)	β (°)	γ (°)	*V* (Å³)	<T1(0)-O> (Å)	<T1(m)-O> (Å)	<T2(0)-O> (Å)	<T2(m)-O> (Å)
untreated		8.1337(3)	12.7822(5)	7.1536(3)	94.257 (3)	116.600(4)	87.823(3)	663.17(5)	1.736	1.610	1.616	1.616
1000	760	8.1493(7)	12.8286(7)	7.1275(4)	93.947(4)	116.508(8)	89.085(5)	665.13(8)	1.693	1.625	1.629	1.629
1000 1060	760 + 670	8.1554 (7)	12.8736(7)	7.1086(4)	93.469(4)	116.436(8)	90.289(5)	666.63(8)	1.647	1.643	1.643	1.642

TABLE 2. Unit-cell parameters of analbite as a function of pressure, determined on the Huber diffractometer

P (GPa)	*V* (Quartz)	*a* (Å)	*b* (Å)	*c* (Å)	α (°)	β (°)	γ (°)	*V* (Å³)
0.0001	113.005(8)	8.1577(5)	12.8753(3)	7.1108(4)	93.487(5)	116.448(4)	90.267(3)	667.04(5)
0.189(5)	112.445(8)	8.1434(6)	12.8656(3)	7.1043(6)	93.521(6)	116.459(5)	90.284(4)	664.65(7)
0.567(6)	111.365(12)	8.1146(5)	12.8464(3)	7.0925(4)	93.585(5)	116.488(5)	90.315(3)	659.98(5)
0.959(5)	110.321(9)	8.0862(5)	12.8270(3)	7.0805(4)	93.626(5)	116.510(5)	90.345(4)	655.38(5)
1.294(5)	109.479(9)	8.0633(6)	12.8121(4)	7.0718(5)	93.653(6)	116.536(6)	90.386(4)	651.77(6)
1.696(6)	108.522(10)	8.0363(6)	12.7935(4)	7.0593(6)	93.693(6)	116.538(5)	90.419(4)	647.43(7)
1.909(5)	108.038(9)	8.0225(5)	12.7853(3)	7.0542(4)	93.710(4)	116.544(4)	90.437(3)	645.39(4)
2.240(5)	107.311(7)	8.0010(4)	12.7706(3)	7.0448(3)	93.726(4)	116.549(4)	90.466(3)	642.00(4)
2.547(6)	106.665(8)	7.9820(5)	12.7582(4)	7.0362(5)	93.745(5)	116.549(5)	90.491(4)	639.05(6)
2.797(7)	106.158(11)	7.9654(4)	12.7479(3)	7.0298(4)	93.744(5)	116.551(4)	90.516(3)	636.58(5)
3.260(5)	105.256(8)	7.9369(5)	12.7289(3)	7.0173(4)	93.767(5)	116.545(4)	90.558(3)	632.23(5)
3.758(6)	104.339(8)	7.9078(6)	12.7098(4)	7.0049(4)	93.772(6)	116.537(6)	90.603(4)	627.88(5)
4.614(7)	102.874(8)	7.8576(4)	12.6775(3)	6.9841(4)	93.771(4)	116.514(4)	90.672(3)	620.54(5)
5.339(8)	101.728(10)	7.8170(7)	12.6520(4)	6.9681(5)	93.770(7)	116.501(6)	90.733(5)	614.71(6)
5.535(7)	101.430(8)	7.8065(5)	12.6448(3)	6.9630(5)	93.771(5)	116.482(4)	90.747(3)	613.18(5)
5.844(7)	100.974(8)	7.7890(7)	12.6330(4)	6.9572(10)	93.753(7)	116.479(7)	90.776(5)	610.75(10)
7.068(7)	99.280(7)	7.7228(5)	12.5901(4)	6.9272(5)	93.771(6)	116.388(5)	90.874(4)	601.30(5)
7.528(8)	98.687(8)	7.6967(5)	12.5727(3)	6.9157(6)	93.769(6)	116.350(5)	90.919(4)	597.63(6)
7.927(9)	98.188(9)	7.6754(7)	12.5592(5)	6.9051(6)	93.769(8)	116.306(7)	90.963(5)	594.62(7)
8.275(8)	97.766(6)	7.6545(6)	12.5471(4)	6.8963(8)	93.788(6)	116.260(6)	91.004(4)	591.87(7)
8.710(8)	97.253(7)	7.6266(6)	12.5309(3)	6.8806(5)	93.797(6)	116.174(6)	91.079(4)	587.99(5)

TABLE 3. Unit-cell parameters and refinement details of analbite at different pressures (σP = 0.1 GPa)

P (GPa)	0.0001*	0.0001	1.2	3.2	5.5	7.2	8.0	9.0	9.4
a (Å)	8.1554(7)	8.1601(11)	8.0813(17)	7.9499(15)	7.8171(14)	7.7267(16)	7.686(2)	7.6155(19)	7.585(2)
b (Å)	12.8736(7)	12.859(5)	12.8061(8)	12.7297(7)	12.660(7)	12.565(6)	12.534(6)	12.538(7)	12.516(7)
c (Å)	7.1086(4)	7.0939(13)	7.073(2)	7.019(2)	6.9517(19)	6.9109(19)	6.883(2)	6.8506(19)	6.8410(19)
α (°)	93.469(4)	93.27(4)	93.549(17)	93.740(10)	93.80(5)	93.52(4)	93.66(5)	93.62(5)	93.58(5)
β (°)	116.436(8)	116.335(16)	116.55(3)	116.55(2)	116.50(2)	116.46(2)	116.25(3)	116.04(3)	115.97(3)
γ (°)	90.289(5)	90.24(3)	90.337(12)	90.510(10)	90.86(4)	90.89(3)	90.74(4)	90.89(4)	91.00(5)
V (Å³)	666.63(8)	665.7(3)	653.1(2)	633.4(2)	613.6(4)	598.8(3)	592.9(4)	585.9(4)	582.0(4)
Refl. Tot.	4886	2785	2677	2404	989	911	2072	1433	1616
Refl. Unique	2209	693	690	641	387	396	557	403	471
Refl. $F_o > 4\sigma(F_o)$	1849	493	520	470	260	302	372	306	287
Refined param.	118	58	58	58	58	58	58	58	58
R (%) $F_o > 4\sigma(F_o)$	4.07	7.35	7.62	7.19	8.02	7.25	12.44	12.30	15.13
wR^2 (%) $F_o > 4\sigma(F_o)$	10.58	17.90	21.40	16.99	18.75	17.39	27.48	29.03	34.06
Goodness of fit	1.00	1.07	1.19	1.48	1.26	1.05	1.05	1.10	1.43

* Reflection intensities collected from a crystal in air.

parameters determined from the CCD data sets (Table 3) were used in the structure model for refinements. Test refinements with cell parameters interpolated from the data collected on the Huber diffractometer (Table 2) yielded bond lengths and angles that are same to within a fraction of the e.s.d. values. Details of the data collections and refinements are reported in Table 3, the atomic coordinates and the thermal parameters are reported in Table 4 and the Na-O and T-O bond lengths are listed in Table 5. The T-O-T and O-T-O angles are reported in Table 6[1] and Table 7[1].

[1] Deposit item AM-11-007, Tables 6 and 7. Deposit items are available two ways: For a paper copy contact the Business Office of the Mineralogical Society of America (see inside front cover of recent issue) for price information. For an electronic copy visit the MSA web site at http://www.minsocam.org, go to the *American Mineralogist* Contents, find the table of contents for the specific volume/issue wanted, and then click on the deposit link there.

TABLE 4. Atomic coordinates and displacement parameters (Å^2) for analbite as a function of pressure (σP = 0.1 GPa)

P (GPa)		0.0001*	0.0001	1.2	3.2	5.5	7.2	8.0	9.0	9.4
Na	*x*	0.2738(2)	0.2744(5)	0.2695(14)	0.2670(15)	0.2602(13)	0.2581(11)	0.2608(11)	0.2544(16)	0.255(3)
	y	0.0078(2)	0.0057(13)	0.0086(8)	0.0095(7)	0.011 (3)	0.006(2)	0.006(2)	0.006(3)	0.009(5)
	z	0.1327(4)	0.1334(9)	0.126(4)	0.134(4)	0.1330(19)	0.1313(15)	0.1323(19)	0.128(3)	0.140(3)
	U_{eq}	0.0961(11)	0.100(12)	0.082(14)	0.097(15)	0.13(3)	0.104(18)	0.08(2)	0.14(3)	0.18(4)
T1(0)	*x*	0.0090(1)	0.0094(2)	0.0084(5)	0.0056(6)	0.0058(6)	0.0047(5)	0.0041(6)	0.0049(8)	0.0054(9)
	y	0.1650(1)	0.1655(6)	0.1635(2)	0.1609(2)	0.1595(12)	0.1586(9)	0.1580(10)	0.1553(12)	0.1513(13)
	z	0.2147(1)	0.2158(3)	0.2146(12)	0.2105(13)	0.2129(7)	0.2128(6)	0.2128(6)	0.2135(8)	0.2150(8)
	U_{iso}	0.0096(2)	0.008(1)	0.015(1)	0.011(1)	0.015(1)	0.017(1)	0.018(1)	0.023(2)	0.021(1)
T1(m)	*x*	0.0047(1)	0.0051(2)	0.0044(5)	0.0018(6)	0.0011(6)	–0.0008(5)	–0.0002(6)	0.0004(8)	0.0011(8)
	y	0.8146(1)	0.8140(6)	0.8145(2)	0.8147(2)	0.8149(12)	0.8134(9)	0.8128(9)	0.8125(11)	0.8120(12)
	z	0.2287(1)	0.2282(3)	0.2311(13)	0.2282(13)	0.2293(7)	0.2285(6)	0.2277(6)	0.2266(7)	0.2267(7)
	U_{iso}	0.0139(2)	0.012(1)	0.015(1)	0.016(1)	0.016(1)	0.016(1)	0.018(1)	0.020(2)	0.017(1)
T2(0)	*x*	0.6904(1)	0.6901(2)	0.6884(5)	0.6843(7)	0.6814(6)	0.6807(6)	0.6802(6)	0.6796(9)	0.6777(9)
	y	0.1080(1)	0.1083(5)	0.1071(2)	0.1051(2)	0.1038(11)	0.1018(9)	0.1014(10)	0.0993(13)	0.0981(13)
	z	0.3205(1)	0.3211(3)	0.3199(12)	0.3161(15)	0.3133(7)	0.3136(6)	0.3140(6)	0.3136(8)	0.3134(8)
	U_{iso}	0.0140(2)	0.013(1)	0.014(1)	0.014(1)	0.017(1)	0.019(1)	0.020(1)	0.025(2)	0.021(1)
T2(m)	*x*	0.6849(1)	0.6849(2)	0.6796(6)	0.6722(7)	0.6653(6)	0.6604(5)	0.6578(7)	0.6569(9)	0.6553(8)
	y	0.8776(1)	0.8780(5)	0.8773(2)	0.8754(2)	0.8753(11)	0.8731(8)	0.8732(10)	0.8723(12)	0.8718(12)
	z	0.3535(1)	0.3526(3)	0.3498(13)	0.3500(16)	0.3525(7)	0.3513(6)	0.3504(6)	0.3499(8)	0.3500(8)
	U_{iso}	0.0137(2)	0.013(1)	0.015(1)	0.014(1)	0.016(1)	0.018(1)	0.022(1)	0.027(2)	0.020(1)
OA(1)	*x*	0.0052(3)	0.0048(7)	0.0032(13)	0.0047(13)	0.0053(17)	0.0046(14)	0.0048(16)	0.004(2)	0.001(3)
	y	0.1347(2)	0.1342(14)	0.1336(5)	0.1323(5)	0.132(3)	0.129(2)	0.127(2)	0.129(2)	0.126(3)
	z	0.9845(3)	0.9850(8)	0.981(2)	0.980(2)	0.9793(18)	0.9777(15)	0.9775(15)	0.9775(19)	0.975(2)
	U_{iso}	0.0226(4)	0.021(1)	0.023(2)	0.023(2)	0.029(3)	0.024(2)	0.029(3)	0.037(4)	0.037(5)
OA(2)	*x*	0.5913(2)	0.5891(7)	0.5864(14)	0.5744(15)	0.5653(15)	0.5628(13)	0.5595(16)	0.554(2)	0.552(2)
	y	0.9906(1)	0.9900(16)	0.9909(5)	0.9885(5)	0.9866(14)	0.9851(13)	0.9877(13)	0.9858(16)	0.9847(16)
	z	0.2781(3)	0.2772(8)	0.282(3)	0.272(3)	0.2741(18)	0.2742(15)	0.2753(17)	0.273(2)	0.272(2)
	U_{iso}	0.0186(4)	0.020(1)	0.020(2)	0.016(1)	0.022(2)	0.024(2)	0.023(2)	0.026(3)	0.027(3)
OB(0)	*x*	0.8213(3)	0.8220(7)	0.8231(16)	0.8162(15)	0.8170(14)	0.8181(14)	0.8145(19)	0.826(2)	0.823(3)
	y	0.1083(2)	0.1090(15)	0.1037(5)	0.0979(5)	0.092(3)	0.083(2)	0.084(2)	0.077(3)	0.073(3)
	z	0.1990(3)	0.2002(8)	0.204(3)	0.190(3)	0.1928(19)	0.1920(16)	0.190(2)	0.203(3)	0.201(3)
	U_{iso}	0.0230(4)	0.021(1)	0.023(2)	0.020(2)	0.026(3)	0.036(3)	0.049(4)	0.063(6)	0.056(6)
OB(m)	*x*	0.8183(3)	0.8192(7)	0.8087(15)	0.8107(17)	0.8017(17)	0.8020(15)	0.801(2)	0.800(3)	0.796(3)
	y	0.8472(2)	0.8441(15)	0.8467(5)	0.8448(6)	0.841(3)	0.841(3)	0.840(4)	0.832(4)	0.828(5)
	z	0.2451(3)	0.2463(9)	0.227(3)	0.246(4)	0.239(2)	0.2417(16)	0.240(2)	0.243(3)	0.240(3)
	U_{iso}	0.0255(4)	0.024(1)	0.021(2)	0.024(2)	0.026(3)	0.030(2)	0.039(3)	0.057(6)	0.043(5)
OC(0)	*x*	0.0159(2)	0.0150(7)	0.0133(14)	0.0010(15)	–0.0088(15)	–0.0171(12)	–0.0179(14)	–0.0224(19)	–0.025(2)
	y	0.2905(2)	0.2916(15)	0.2884(5)	0.2871(5)	0.2857(15)	0.2845(14)	0.2836(14)	0.2820(16)	0.2780(16)
	z	0.2769(3)	0.2735(8)	0.285(3)	0.278(3)	0.2734(18)	0.2734(13)	0.2744(17)	0.270(2)	0.275(2)
	U_{iso}	0.0207(4)	0.019(1)	0.017(1)	0.022(2)	0.023(3)	0.024(2)	0.024(2)	0.028(3)	0.025(3)
OC(m)	*x*	0.0210(3)	0.0208(7)	0.0179(15)	0.0144(17)	0.0105(16)	0.0143(14)	0.0130(17)	0.014(2)	0.007(2)
	y	0.6872(2)	0.6845(17)	0.6867(5)	0.6855(6)	0.6861(16)	0.6851(14)	0.6846(15)	0.6837(16)	0.6822(17)
	z	0.2181(3)	0.2191(9)	0.214(4)	0.207(4)	0.2017(19)	0.2031(15)	0.2016(17)	0.198(2)	0.200(2)
	U_{iso}	0.0217(4)	0.021(1)	0.024(2)	0.027(2)	0.027(3)	0.028(2)	0.028(3)	0.037(4)	0.027(4)
OD(0)	*x*	0.1956(2)	0.1953(7)	0.1990(13)	0.2027(14)	0.2071(14)	0.2102(15)	0.211(2)	0.210(3)	0.223(3)
	y	0.1122(1)	0.1062(15)	0.1120(6)	0.1119(5)	0.110(3)	0.114(2)	0.113(3)	0.109(4)	0.114(5)
	z	0.3876(3)	0.3875(8)	0.387(2)	0.387(3)	0.3873 (16)	0.3865(15)	0.3856(17)	0.386(2)	0.386(2)
	U_{iso}	0.0204(4)	0.020(1)	0.027(2)	0.021(2)	0.023(3)	0.031(2)	0.039(3)	0.048(5)	0.055(6)
OD(m)	*x*	0.1887(3)	0.1885(7)	0.1864(13)	0.1886(13)	0.1925(16)	0.1879(13)	0.1901(16)	0.191(2)	0.194(2)
	y	0.8674(2)	0.8660(16)	0.8670(6)	0.8679(6)	0.867(3)	0.871(2)	0.864(3)	0.869(3)	0.867(4)
	z	0.4262(3)	0.4238(9)	0.420(2)	0.425(2)	0.4321(17)	0.4321(14)	0.4296(17)	0.430(2)	0.431(2)
	U_{iso}	0.0226(4)	0.023(1)	0.026(2)	0.023(2)	0.029(3)	0.032(2)	0.030(3)	0.046(5)	0.041(5)

Note: The Na sites were refined with anisotropic displacement parameters at all pressures, and the equivalent isotropic parameters (U_{eq}) are reported here.
* Reflection intensities collected from a crystal in air: all the sites were refined with anisotropic displacement parameters and the equivalent isotropic parameters (U_{eq}) are reported here.

TABLE 5. Na-O and T-O bond distances (Å) for analbite as a function of pressure (σP = 0.1 GPa)

P(GPa)	0.0001*	0.0001	1.2	3.2	5.5	7.2	8.0	9.0	9.4
Na-OA(1)	2.601(3)	2.618(18)	2.553(16)	2.494(14)	2.43(3)	2.41(2)	2.40(3)	2.37(3)	2.35(4)
Na-OA(1)	2.706(3)	2.688(16)	2.653(12)	2.600(13)	2.54(4)	2.44(3)	2.43(3)	2.40(4)	2.37(6)
Na-OA(2)	2.339(2)	2.320(7)	2.311(15)	2.216(15)	2.172(13)	2.138(10)	2.082(13)	2.080(17)	2.066(19)
Na-OB(0)	2.516(3)	2.516(15)	2.46(3)	2.39(3)	2.36(3)	2.26(2)	2.25(2)	2.25(3)	2.30(3)
Na-OB(m)	3.176(4)	3.22(2)	3.04(3)	3.18(3)	3.16(4)	3.18(3)	3.18(4)	3.24(6)	3.29(7)
Na-OC(0)	3.373(3)	3.32(2)	3.402(18)	3.360(13)	3.36(4)	3.27(3)	3.26(3)	3.28(4)	3.34(5)
Na-OC(m)	2.909(3)	2.90(2)	2.877(12)	2.831(13)	2.80(4)	2.84(3)	2.82(3)	2.83(4)	2.75(6)
Na-OD(0)	2.498(3)	2.472(13)	2.476(19)	2.38(2)	2.29(3)	2.32(2)	2.30(2)	2.27(3)	2.18(4)
Na-OD(m)	3.136(4)	3.107(18)	3.13(3)	3.07(2)	3.06(4)	2.99(3)	3.01(4)	2.96(5)	2.93(6)
<Na-O>	2.806	2.796	2.767	2.724	2.687	2.650	2.635	2.630	2.620
T1(0)-OA(1)	1.6458(19)	1.648(7)	1.657(14)	1.630(14)	1.636(14)	1.643(11)	1.644(10)	1.628(12)	1.640(14)
T1(0)-OB(0)	1.648(2)	1.646(10)	1.647(7)	1.645(7)	1.640(17)	1.658(17)	1.656(18)	1.636(19)	1.64(2)
T1(0)-OC(0)	1.6433(19)	1.64(2)	1.641(7)	1.650(9)	1.645(18)	1.642(16)	1.635(16)	1.649(18)	1.658(18)
T1(0)-OD(0)	1.6537(19)	1.686(11)	1.650(12)	1.662(12)	1.665(14)	1.642(10)	1.643(14)	1.636(16)	1.643(17)
<T1(0)-O>	1.648	1.656	1.649	1.647	1.646	1.646	1.644	1.637	1.646
T1(m)-OA(1)	1.656(2)	1.657(10)	1.652(14)	1.632(13)	1.616(15)	1.624(13)	1.628(16)	1.607(17)	1.619(18)
T1(m)-OB(m)	1.631(2)	1.624(8)	1.626(7)	1.624(7)	1.628(11)	1.608(8)	1.607(11)	1.599(13)	1.616(14)
T1(m)-OC(m)	1.646(2)	1.67(2)	1.641(7)	1.650(8)	1.635(18)	1.623(18)	1.614(17)	1.625(18)	1.627(18)
T1(m)-OD(m)	1.6384(19)	1.629(10)	1.589(12)	1.613(14)	1.620(16)	1.624(15)	1.598(15)	1.619(17)	1.621(17)
<T1(m)-O>	1.643	1.645	1.627	1.630	1.625	1.620	1.612	1.613	1.621
T2(0)-OA(2)	1.6563(19)	1.67(2)	1.644(7)	1.655(8)	1.669(17)	1.657(16)	1.632(16)	1.638(17)	1.632(18)
T2(0)-OB(0)	1.645(2)	1.648(5)	1.630(12)	1.644(11)	1.622(11)	1.632(10)	1.614(12)	1.621(15)	1.625(16)
T2(0)-OC(m)	1.6387(19)	1.611(15)	1.640(12)	1.631(11)	1.642(15)	1.611(12)	1.611(13)	1.616(15)	1.630(15)
T2(0)-OD(m)	1.631(2)	1.644(7)	1.664(15)	1.644(14)	1.608(12)	1.601(10)	1.621(10)	1.610(12)	1.609(13)
<T2(0)-O>	1.643	1.644	1.645	1.643	1.635	1.625	1.620	1.621	1.624
T2(m)-OA(2)	1.6518(19)	1.64(2)	1.640(10)	1.649(8)	1.627(16)	1.612(15)	1.635(15)	1.638(16)	1.631(17)
T2(m)-OB(m)	1.626(2)	1.631(8)	1.663(11)	1.611(11)	1.632(12)	1.628(9)	1.635(11)	1.628(14)	1.632(15)
T2(m)-OC(0)	1.641(2)	1.642(14)	1.636(7)	1.630(9)	1.626(15)	1.623(14)	1.619(15)	1.632(16)	1.665(17)
T2(m)-OD(0)	1.6510(19)	1.659(6)	1.670(15)	1.654(15)	1.625(11)	1.629(10)	1.638(11)	1.639(14)	1.626(15)
<T2(m)-O>	1.643	1.644	1.652	1.636	1.628	1.623	1.631	1.634	1.639

* Reflection intensities collected from a crystal in air.

RESULTS AND DISCUSSION

Equation of state

No discontinuities were present in either the variation of the volume or the unit-cell parameters with pressure up to the maximum pressure achieved of 8.710(8) GPa. It is clear from the volume-pressure data (Fig. 1a) that the compression of analbite is similar to that of low albite at low pressures but diverges at higher pressures. When the *P-V* data are reformulated as an *f-F* plot (Angel 2000), the data points of analbite show a strong curvature (Fig. 1b), similar to low albite, which means that the data can only be fit with a fourth-order equation of state. The refined equation of state parameters to these data are K_{0T} = 50.3(5) GPa, K_0' = 8.9(5), and K_0'' = –2.4(3) GPa^{-1}. The value of the room-pressure bulk modulus of analbite is thus ~4% lower than that of low albite (Benusa et al. 2005) suggesting that increasing disorder causes the structure of albite to become more compressible at low pressures. This contradicts the study of high albite by Tenner et al. (2007) in which the data were fit to a third-order equation of state and yielded a bulk modulus of 56.4(7) GPa, stiffer than low albite. However, the data of Tenner et al. (2007) are significantly scattered (Fig. 1b), and do not extend to either low or high pressures so they do not exclude the possibility that the true equation of state is of fourth-order, which would inevitably have a lower value of K_{0T} than they reported. The slope of the *f-F* plot (Fig. 1b) is a function of (K' – 4), so the negative slope for our analbite data at higher pressures indicates that K' is decreasing and this eventually leads to $K' = dK/dP < 0$ and thus indicates elastic softening at higher pressures. The same is apparent in the plot (Fig. 1c) of the bulk moduli of the two phases, as derived from the refined fourth-order Birch-Murnaghan EoS. At lower pressures the bulk modulus of analbite is slightly but significantly less than that of albite. But at about 3 GPa, the moduli of the two phases become equal and the subsequent softening of albite above 5 GPa (from the top of the dotted curve in Fig. 1c) means that the analbite is much stiffer at higher pressures, even though softening also starts in analbite at approximately 6.7 GPa (Fig. 1c).

Anisotropy of compression

The *b* and *c* unit-cell parameters show a significantly greater fractional decrease in analbite than in low albite but the *a*-axis is softer in low albite than in analbite (Fig. 2), immediately indicating that the compressional anisotropy of analbite is less than that of albite. The biggest difference in the unit-cell parameters of albite and analbite at room pressure is in the unit-cell angles, as a consequence of the spontaneous strain arising from the change in the state of order (e.g., Salje 1985; Kroll et al. 1986). As a consequence, there are significant differences in the evolution of the unit-cell angles of the two phases with pressure (Fig. 3). The unit-cell angle α of low albite shows a decrease with pressure while for analbite it shows an increase. Around 8 GPa, both have nearly the same angle (Fig. 3), while the evolution of the unit-cell angles β and γ of analbite approximately parallels that of albite to this pressure. The divergence of the β and γ angles at higher pressures is associated with the softening in albite (Fig. 1c).

For a triclinic mineral, the complete description of the deformation of the unit cell is provided by the strain ellipsoid that represents, in this case, the shape a sphere made of the crystal would become after hydrostatic compression. The magnitudes

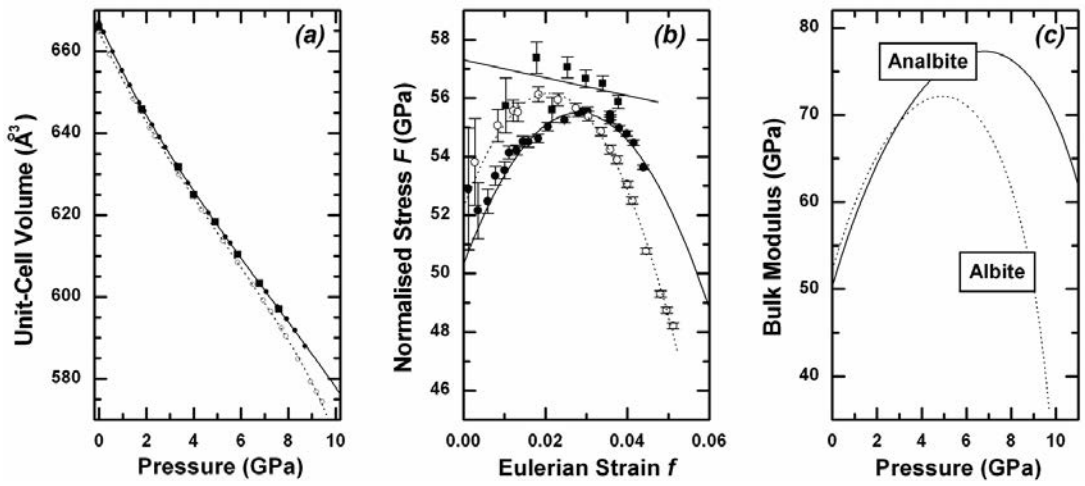

Figure 1. The pressure-volume data and equations of state of albite (Benusa et al. 2005; open circles and dashed lines), high albite (Tenner et al. 2007; filled squares), and analbite (this work; filled circles and solid lines). Lines are fourth-order Birch-Murnaghan equations of state for analbite and low albite and a third-order Birch-Murnaghan equation of state for the high albite data of Tenner et al. (2007). (**a**) Pressure-volume plot. Experimental uncertainties are smaller than symbols. (**b**) The *f-F* plot. (**c**) The variation of the bulk moduli of albite and analbite as a function of pressure derived from the fits of the Birch-Murnaghan fourth-order equations of state to the *P-V* data.

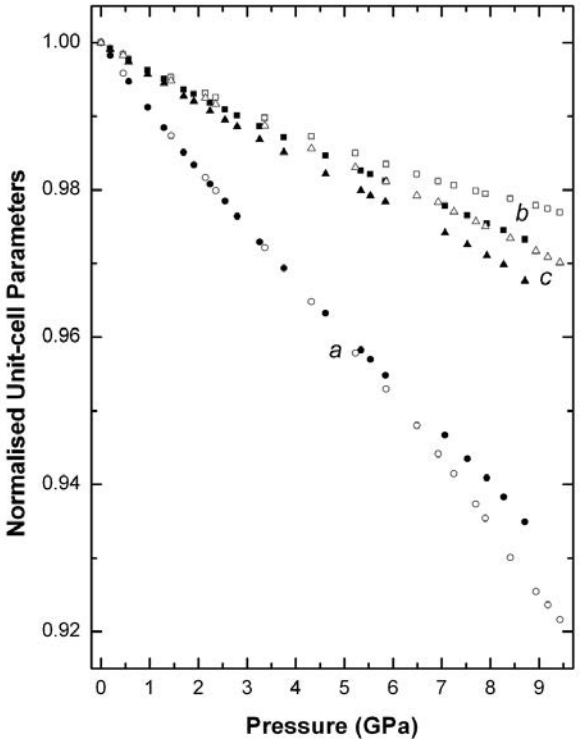

Figure 2. Fractional changes of the unit-cell edges with pressure of analbite (solid symbols) and low albite (Benusa et al. 2005; open symbols). Experimental uncertainties are smaller than symbols.

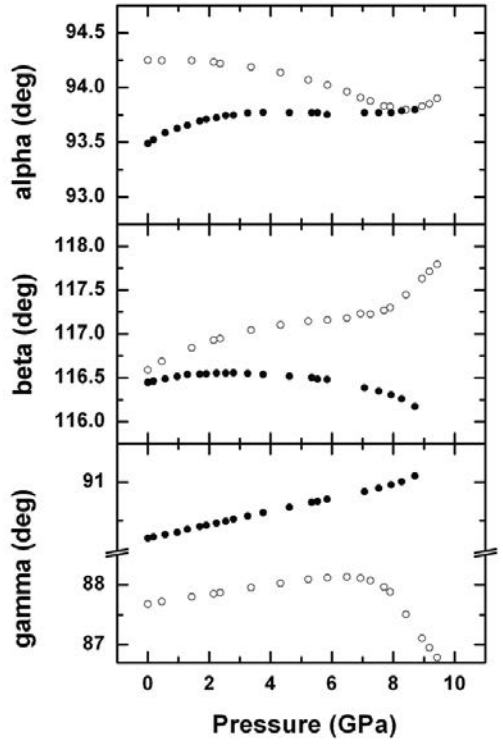

Figure 3. Variation of the unit-cell angles with pressure of analbite (solid symbols) and low albite (Benusa et al. 2005; open symbols). Experimental uncertainties are smaller than symbols.

and orientations of the principal axes of the strain ellipsoid, calculated from the cell parameters of Table 2 with the STRAIN program (Ohashi 1982), are reported in Table 8 and are compared with the results of Benusa et al. (2005) for low albite over the entire pressure range. As for other feldspars, the compression of analbite is anisotropic, with 55% of the total compression accommodated along ε_1. However, this anisotropy is significantly less than that in albite, in which ε_1 accounts for 62% of the compression over the pressure range 0.0001–8.4 GPa (Benusa et al. 2005), but is similar to that of anorthoclase (Nestola et al.

TABLE 8. Linear axial compressibilities ($\times 10^{-3}$ GPa^{-1}), magnitudes ($\times 10^{-3}$ GPa^{-1}), and orientations of the principal axes of the strain ellipsoids for analbite and low albite

	P range (GPa)	β_a	β_b	β_c		Unit strain	Angle (°) with			$\varepsilon_1/(\varepsilon_1+\varepsilon_2+\varepsilon_3)$
							a	*b*	*c*	
Analbite	0–8.71	7.47	3.07	3.72	ε_1	7.8 (1)	16	80	105	55%
					ε_2	3.8 (1)	106	59	36	
					ε_3	2.6 (1)	93	33	122	
Low albite	0–8.41	8.32	2.52	3.16	ε_1	9.2	23	92	94	62%
Benusa et al. (2005)					ε_2	3.4	111	121	27	
					ε_3	2.2	98	31	64	

Note: The compressibilities were calculated as $-\beta = [(d - d_0)/d_0]/P$ where d is a unit-cell parameter.

2008). The evolution of the orientation of the principal axes ε_1, ε_2, and ε_3 of the strain ellipsoid of analbite with pressure (Fig. 4) also differs significantly from albite with the major axis ε_1 moving closer to the [100] direction with increasing pressure, while in low albite it remains closer to *a**.

Crystal structure evolution

In analbite the average bond lengths of the four tetrahedra (Table 5) exhibit only very small changes with increasing pressure. The major changes in the structures of both analbite and low albite (Benusa et al. 2005) upon compression are therefore due to the flexing of the T-O-T bond angles with the tetrahedral units remaining essentially rigid (Tables 6[1] and 7[1]). In analbite the variation of the T-O-T angles (Table 6[1]) is definitely less than in low albite (Fig. 5), and indeed reflects the trends shown in low albite between 0.0001 and 4 GPa, and do not show the change in behavior found in low albite at pressures above 5 GPa. As a consequence, the O-O-O angles of the T1(0)-T2(0)-T1(m)-T2(m) four-membered rings of tetrahedra parallel to (010) (Fig. 6) show no significant shear in analbite, while the shear of the same rings in ordered albite is clearly evident at 9.4 GPa (Figs. 6 and 7). The significant rotation of both T1 tetrahedra around the [001] direction observed by Benusa et al. (2005) in low albite is observable also in analbite, but the changes are definitely lower.

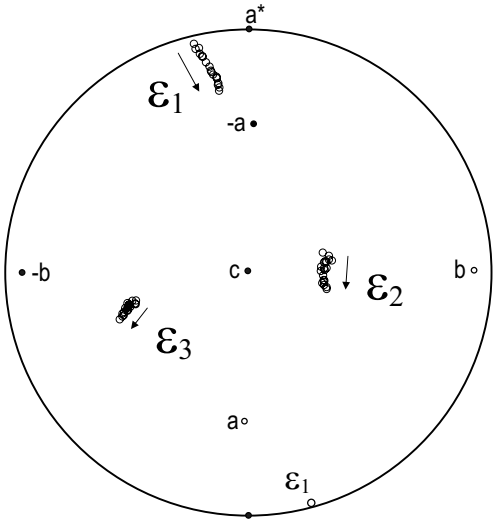

FIGURE 4. Stereographic projection showing the orientation of the principal axes, ε_1, ε_2, ε_3, of the strain ellipsoid describing the unit-cell compression of analbite (*P* range = 1 atm–8.7 GPa). All three poles are plotted in the upper hemisphere. The direct lattice vectors and the **a*** reciprocal vector of analbite at room pressure are shown; +**a** and +**b** are plotted in the lower hemisphere.

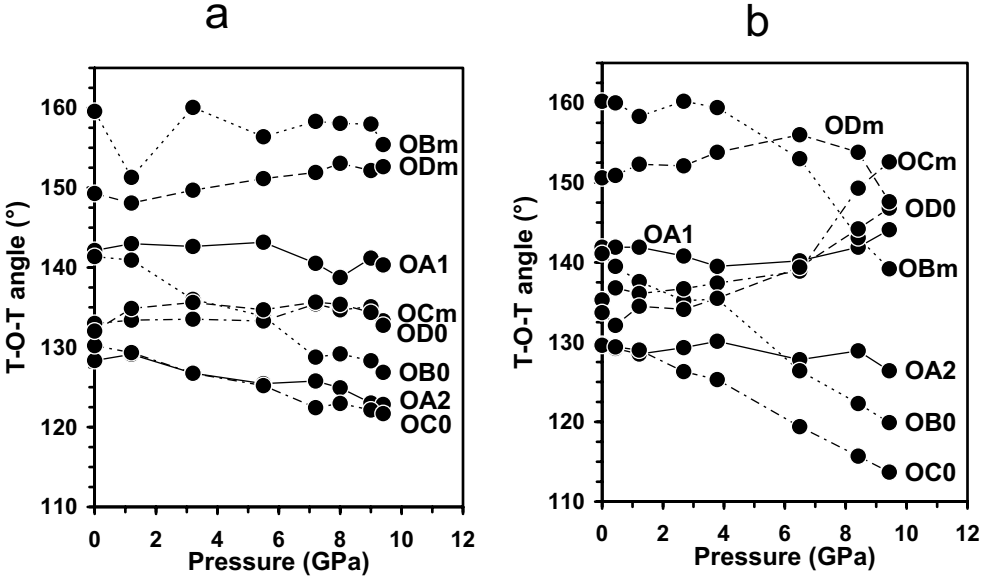

FIGURE 5. The evolution of the T-O-T angles with pressure in (**a**) analbite and (**b**) low albite (Benusa et al. 2005). Distinct line types link the data for OA, OB, OC, OD atoms. Experimental uncertainties are between 0.1 and 2°.

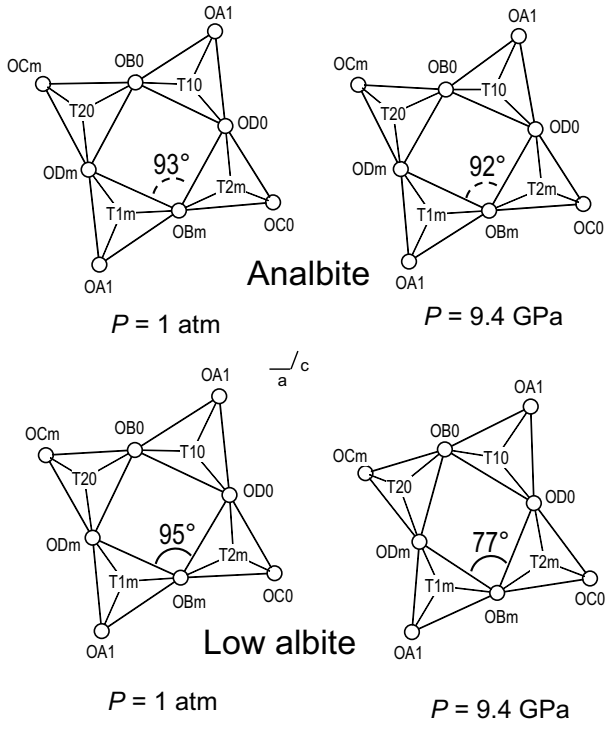

FIGURE 6. The four-membered tetrahedral ring of the crankshaft chain, with (010) as the ring-plane. Projection on the *a*-*c* plane (thickness ~3 Å) at $P = 1$ atm and at $P = 9.4$ GPa in analbite and in low albite (Downs et al. 1994; Benusa et al. 2005). The ring consists of four symmetrically distinct tetrahedra. Apical O atoms are not shown. The values of the OD-OB-OD angles are indicated.

The rotations observed for the T1(m) and T1(0) tetrahedra do not exceed 3 and 7°, respectively, in analbite.

The anisotropy of compression of analbite is due to the softness of the *a* unit-cell parameter and the d_{100} plane spacing that, as in all feldspars, is due to the intrinsic flexibility of the crankshaft chains of tetrahedra that allows them to be compressed. Even though the compression of the *a* parameter is less in analbite than in low albite ($\Delta a = -0.53$ Å for analbite, $\Delta a = -0.60$ Å for low albite to ~8.7 GPa), the evolution of the OC(0)-OA(1) and OC(0)-OC(m) distances (Fig. 8) across the channels spanned by the crankshaft chains clearly shows the considerable narrowing of the chains, even in the absence of shear of the (010) tetrahedral rings. Obviously, the narrowing is significantly higher in low albite in the presence of the ring shear. The *b* parameter shows a slightly higher compressibility in analbite than in low albite (for analbite $\Delta b = -0.34$ Å, for albite $\Delta b = -0.28$ Å to ~8.7 GPa), although the O-O-O angles are more flexible in low albite (Fig. 7b). The variations of the OD-OC-OD angles with pressure are shown in Figure 9, in which the four-membered rings parallel to the $(10\bar{1})$ plane, forming the sides of the chains of the crankshaft, are projected at $P = 9.4$ GPa for the two albite structures.

In the Na-polyhedron the shorter Na-O distances (Table 5; Fig. 10a) decrease significantly in analbite, while the longer Na-O distances do not show significant differences with pressure. In particular, the Na-OB(0) and Na-OD(0) bond lengths oriented along the shorter diagonal of the OB(0)-OD(m)-OD(0)-OB(m) quadrilateral (Fig. 11), which lies in the (100) plane, and the Na-OA2 and Na-OA1 distances in the plane *b*-*a** decrease dramatically. The Na displacement ellipsoid is elongated along the longest diagonal OD(m)-OB(m) of the OB(0)-OD(m)-OD(0)-OB(m) quadrilateral. The variation of Na-O bond lengths with pressure suggests that the coordination number of Na in

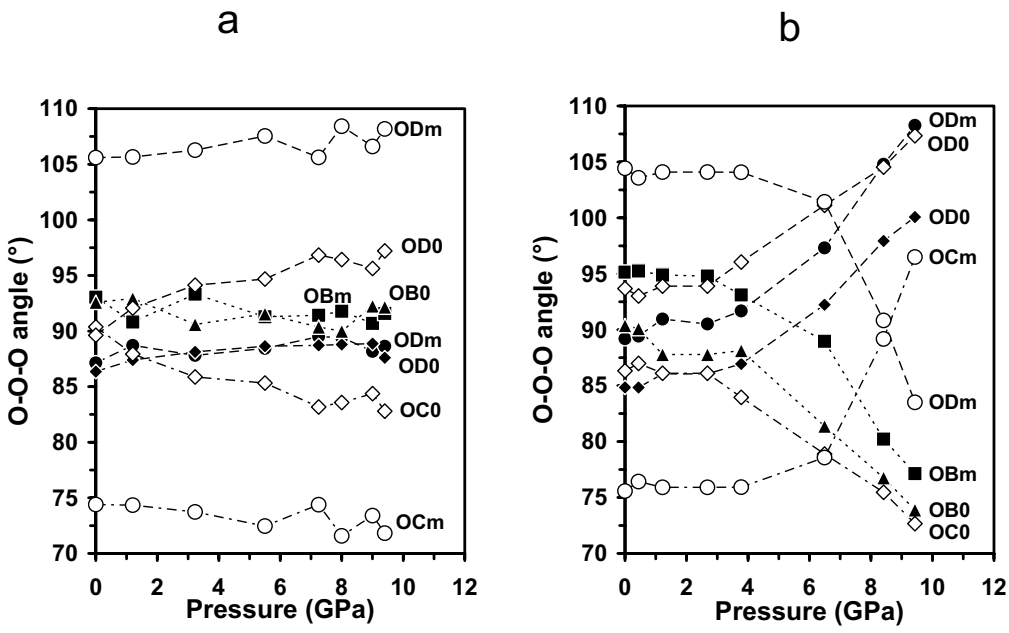

FIGURE 7. The O-O-O angle variations vs. pressure in (**a**) analbite and (**b**) low albite (Benusa et al. 2005). Solid symbols are the four internal angles of the OB(0)-OD(m)-OB(m)-OD(0) ring parallel to the (010) plane (denoted ring 1 in Benusa et al. 2005) and open symbols are the angles of the rings parallel to the $(10\bar{1})$ plane (denoted rings 2 and 3 in Benusa et al. 2005). Experimental uncertainties are between 0.2 and 2°.

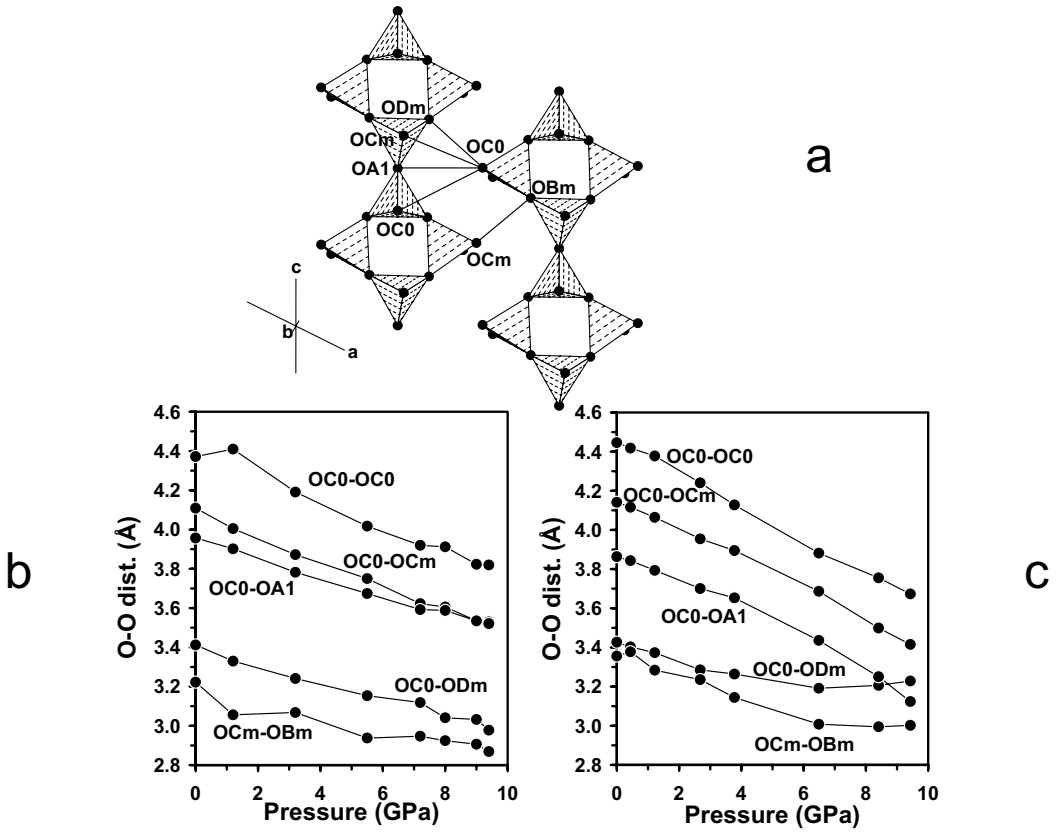

FIGURE 8. (**a**) Polyhedral representation of analbite at room pressure projected down the [010] axis. (**b**) Evolution of the O-O distances between the two chains parallel to the [001] axis with pressure in analbite and (**c**) in low albite (Benusa et al. 2005). Experimental uncertainties are between 0.01 and 0.06 Å.

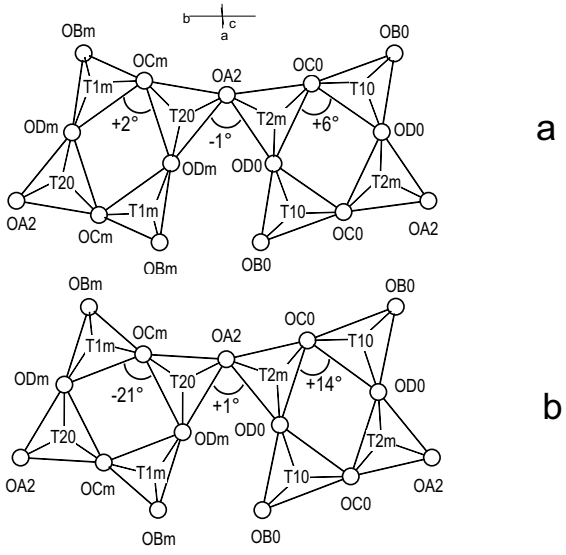

FIGURE 9. The four-membered rings of tetrahedra approximately normal to the *a* axis, with ring-planes near to the (10$\bar{1}$) plane (denoted rings 2 and 3 in Benusa et al. 2005). Apical O atoms are not shown. Projection on to the (10$\bar{1}$) plane (thickness ~3 Å) at P = 9.4 GPa in (**a**) analbite and (**b**) low albite (Benusa et al. 2005). The variations in the OD-OC-OD and OD-OA-OD angles between P = 9.4 GPa and room pressure are indicated.

analbite remains 5 with increasing pressure (Fig. 11). The Na-OA2 distance decreases regularly (within the limits of the high standard deviations at HP). So, as for albite, the "strut" OA(2)-Na-Na-OA(2), that was proposed to be holding the crankshaft chains open (Megaw 1970), thus appears to have a completely passive role in compression, and is slightly shorter in analbite than albite.

The disordering of Al and Si in analbite makes very little difference to the stiffness of the structure (in terms of volume variation) at crustal pressures; analbite is marginally softer than albite (by <4%) up to 3 GPa. The dominant compression mechanism in both minerals is the closing-up of the "crankshaft" chains of tetrahedra, which is the cause of the extreme anisotropy of compression (and thermal expansion) of all feldspars. However, disordering of Al and Si to produce analbite does result in reduced anisotropy of compression compared to albite, and a rotation of the strain ellipsoid from that of albite. This must be due to the redistribution of the Si-O-Si and Al-O-Si links within the structure, and the small consequent changes in individual T-O bond lengths. Whatever the details, the distribution of the different T-O-T linkages must be more isotropic in analbite than albite, and this must be the cause of the reduction in the anisotropy of compression of analbite. The rotation of the strain ellipsoid must be the result of the interaction of these changes with the intrinsic elastic anisotropy and the dominant mode of compression of the

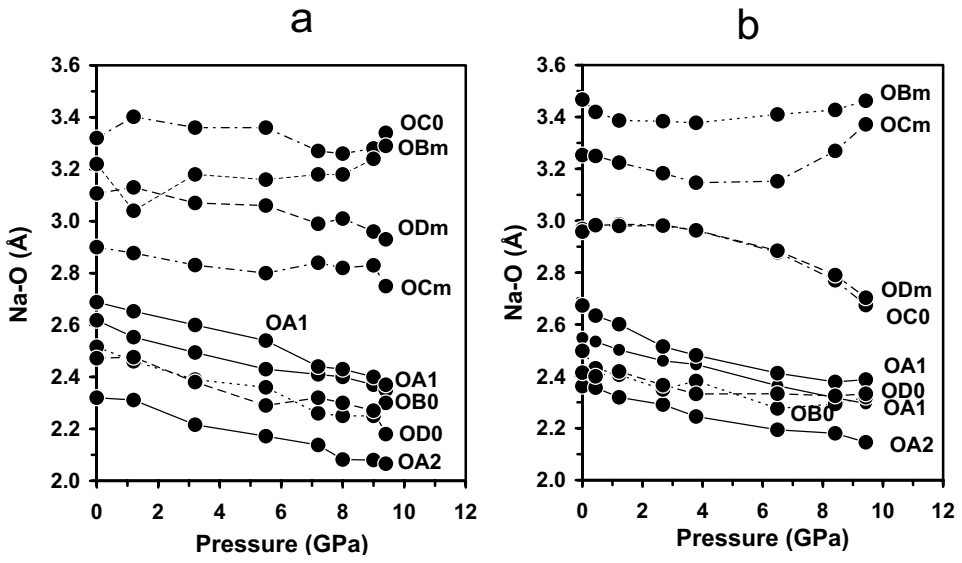

FIGURE 10. Na-O bond length evolution vs. pressure in (**a**) analbite and (**b**) low albite (Benusa et al. 2005). Distinct line types link the data for OA, OB, OC, OD central O atoms. Experimental uncertainties are between 0.002 and 0.07 Å.

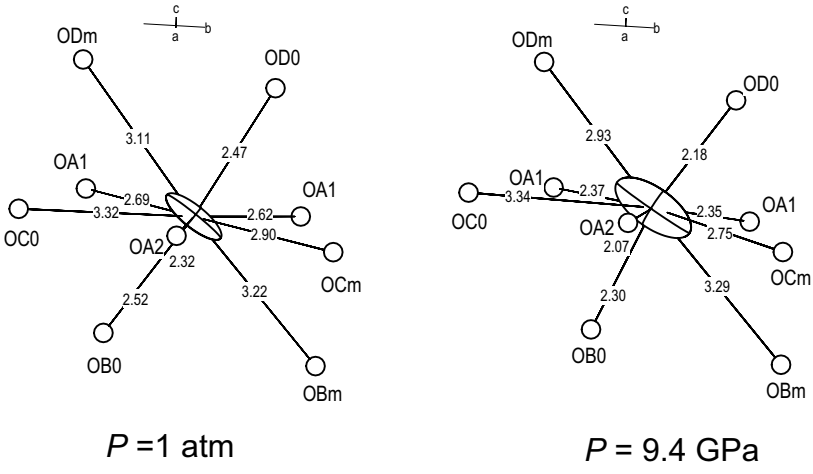

FIGURE 11. The Na-polyhedron in analbite at room pressure (crystal in the DAC) and at P = 9.4 GPa. Projection is near the (100) plane. The Na-O distances (Å) are indicated.

feldspar framework that involves the crankshaft chains and arises simply from its topology.

The unusual feature of the compression of low albite is the softening of the structure that starts at 5 GPa (Fig. 1c) and continues to at least 9.4 GPa (Fig. 1a). This softening was previously attributed to the initiation of the shear of the four-rings of tetrahedra within the structure (Fig. 6). However, an important result from the structural study of analbite is that the ring shear is not observed up to 9.4 GPa, whereas volume softening (the maximum in the *K-P* curve; Fig. 1c) starts at 6.75 GPa. Therefore the ring shear cannot be directly responsible for all of the initial bulk volume softening in feldspars, and the structural cause of this softening will only be identified through further systematic studies of the structural response of feldspars to pressure. What is clear is that the structural evolution of analbite from 0.0001 to 9.4 GPa is very similar, in terms of changes in T-O-T bond angles, to the trends exhibited by albite at lower pressures, before the softening occurs. In this sense, it might be said that analbite shows a significantly greater structural rigidity than low albite over the larger pressure range, even though at low pressures analbite is marginally softer than low albite.

ACKNOWLEDGMENTS

The authors thank associate editor Alexandra Friedrich and two anonymous referees for their critical reading of the manuscript and for helpful suggestions. Equation of state measurements in the VT Crystallography Laboratory were supported by NSF grant EAR-0738692 to N.L. Ross and R.J. Angel, and the College of Science at Virginia Tech. Financial support has been provided by MIUR (Roma): PRIN 200604794 to E. Bruno. The Interdepartmental "Scansetti" and "CrisDi" Centres of Turin University are thanked.

REFERENCES CITED

Angel, R.J. (1994) Feldspars at high pressure. In I. Parsons, Ed., Feldspars and Their Reactions, p. 271–312. Kluwer, Dordrecht, The Netherlands.

——— (2000) Equations of state. In R.M. Hazen and R.T. Downs, Eds., High-

temperature and High-pressure Crystal Chemistry, 41, p. 35–59. Reviews in Mineralogy and Geochemistry, Mineralogical Society of America and Geochemical Society, Chantilly, Virginia.

——— (2004) Absorption corrections for diamond-anvil pressure cells implemented in a software package Absorb-6.0. Journal of Applied Crystallography, 37, 486–492.

Angel, R.J., Allan, D.R., Miletich, R., and Finger, L.W. (1997) The use of quartz as an internal pressure standard in high-pressure crystallography. Journal of Applied Crystallography, 30, 461–466.

Benna, P., Nestola, F., Boffa Ballaran, T., Balić-Žunić, T., Lundegaard, L.F., and Bruno, E. (2007) The high-pressure structural configurations of $Ca_{0.2}Sr_{0.8}Al_2Si_2O_8$ feldspar: the *I*$\bar{1}$-*I*2/*c* and *I*2/*c*-*P*2$_1$/*c* phase transitions. American Mineralogist, 92, 1190–1199.

Benusa, M.D., Angel, R.J., and Ross, N.L. (2005) Compression of albite, $NaAlSi_3O_8$. American Mineralogist, 90, 1115–1120.

Downs, R.T., Hazen, R.M., and Finger, L.W. (1994) The high-pressure crystal chemistry of low albite and the origin of the pressure dependency of Al-Si ordering. American Mineralogist, 79, 1042–1052.

King, H.E. and Finger, L.W. (1979) Diffracted beam crystal centering and its application to high-pressure crystallography. Journal of Applied Crystallography, 12, 374–378.

Kroll, H., Schmiemann, I., and von Cölln, G. (1986) Feldspar solid solutions. American Mineralogist, 71, 1–16.

Mao, H.K., Xu, J., and Bell, P.M. (1986) Calibration of the ruby pressure gauge to 800 kbar under quasi-hydrostatic conditions. Journal of Geophysical Research, 91, 4673–4676.

Megaw, H.D. (1970) Structural relationship between coesite and feldspar. Acta Crystallographica, B26, 261–265.

Miletich, R., Allan, D.R., and Kuhs, W.F. (2000) High pressure single-crystal techniques. In R.M. Hazen and R.T. Downs, Eds., High-temperature and High-pressure Crystal Chemistry, 41, p. 445–519. Reviews in Mineralogy and Geochemistry, Mineralogical Society of America and Geochemical Society, Chantilly, Virginia.

Nestola, F., Curetti, N., Benna, P., Ivaldi, G., Angel, R.J., and Bruno, E. (2008) Compressibility and high-pressure behaviour of $Ab_{63}Or_{27}An_{10}$ anorthoclase. Canadian Mineralogist, 46, 1443–1454.

Ohashi, Y. (1982) A program to calculate the strain tensor from two sets of unit-cell parameters. In R.M. Hazen and L.W. Finger, Eds, Comparative Crystal Chemistry, p. 92–102. Wiley, Chichester.

Quareni, S. and Taylor, W.H. (1971) Anisotropy of the sodium atom in low albite. Acta Crystallographica, B27, 281–285.

Ross, N.L. (2000) Framework structures. In R.M. Hazen and R.T. Downs, Eds., High-Temperature and High-Pressure Crystal Chemistry, 41, p. 257–287. Reviews in Mineralogy and Geochemistry, Mineralogical Society of America and Geochemical Society, Chantilly, Virginia.

Salje, E.K.H. (1985) Thermodynamics of sodium feldspar I: order parameter treatment and strain induced coupling effects. Physics and Chemistry of Minerals, 12, 93–98.

Sheldrick, G.M. (2008) A short history of SHELX. Acta Crystallographica, A64, 112–122.

Smith, J.V. and Brown, W.L. (1988) Feldspar Minerals, 1. Crystal Structures, Physical, Chemical and Microtextural Properties, 2nd ed., p. 828, Springer-Verlag, Berlin.

Tenner, T.J., Lange, R.A., and Downs, R.T. (2007) The albite fusion curve re-examined: new experiments and the high-pressure density and compressibility of high albite and $NaAlSi_3O_8$ liquid. American Mineralogist, 92, 1573–1585.

Winter, J.K., Ghose, S., and Okamura, F.P. (1977) A high-temperature study of the thermal expansion and the anisotropy of the sodium atom in low albite. American Mineralogist, 62, 921–931.

Winter, J.K., Okamura, F.P., and Ghose, S. (1979) A high-temperature structural study of high albite, monalbite, and the analbite-monalbite phase transition. American Mineralogist, 64, 409–423.

Manuscript received May 14, 2010
Manuscript accepted September 14, 2010
Manuscript handled by Alexandra Friedrich